Study of transport properties of $Ge_{50-x}Sb_yTe_{100+x-y}$ thin film alloy

A. A. BAHGAT*
Department of Physics, Faculty of Science(Boys), Al-Azhar University, Nasr City 11884, Cairo, Egypt
E-mail: alaabahgat@yahoo.com

E. A. MAHMOUD, A. S. ABD RABO, I. A. MAHDY
Department of Physics, Faculty of Science(Girls), Al-Azhar University, Nasr City 11884, Cairo, Egypt

Published online: 12 April 2006

The transport properties of $Ge_{50-x}Sb_yTe_{100+x-y}$ Alloys where $0 \leq x \leq 15$ and $0 \leq y \leq 30$ in the thin films state were studied. The temperature dependence of the d.c. electrical conductivity measurements for all prepared composition with different thickness, shows that, all samples behaves as a semiconductor up to a specific temperature at which an abrupt transition appears. That transition is due to the change of the semiconductor from non-degenerate to degenerate state. The temperature dependence of a.c. electrical conductivity measurements shows that, the a.c. conductivity for all films are frequency independent in the tested frequency range from 0.12 to 10 kHz. Thermoelectric power was found to have positive sign indicating that these alloys are p-type semiconductors. The value of temperature coefficient γ was found to be in the order of 10^{-4} (eV/K). The calculation of the free-charge carrier concentration and charge mobility shows that, the abrupt transition appears in thermoelectric power and conductivity are due to an abrupt increase in the mobility.

1. Introduction

Chalcogenide alloys have received considerable attention because of their wide-range of applications in infrared transmission, semiconductors, photovoltaics and in phase change optical recording technology [1, 2]. Chalcogenide materials especially those which having Ge and Te metals have an importance in modern technology, for instance GeTe exhibit high thermal stability of the amorphous phase and also fast crystallization times, which are required for direct optical overwrite process [3]. This indicates that, it can be used as an electrical switch, in memory devices such as CD or DVD, and also this material have high piezoelectricity, which make it applicable in many other applications. Some of the electrical properties for this alloy were reported [4–6]. It is noted that, the addition of antimony to the GeTe binary system increase the practicality of commercial-scale production by easing the requirement for precision in composition of the deposited film without deleterious effects in the speed of stability [7]. On the other hand, if antimony is substituted for germanium, it helps to relax the interatomic stresses between Te and Ge and allowing the formation of a more symmetrical (fcc) structure [7]. Earlier studies revealed that the chalcogenide compounds with stoichiometric composition in the Ge-Sb-Te ternary system are good candidate materials for an active optical recording medium [8, 9]. Kooi *et al*. [10] studied the crystallization of amorphous $Ge_2Sb_2Te_5$ films (10, 40, and 70 nm thick) using in situ heating in a transmission electron microscope (TEM) and found that, the electron irradiation-induced crystallization is possible at room temperature using a 400 kV electron beam. The crystallization kinetics of $Ge_4Sb_1Te_5$ films had been investigated by Wamwangi *et al*. [11] and found that, these systems has a cubic structure after crystallization.

The aim of the present work is to extend the study of the transport properties of Ge-Te and Ge-Sb-Te system.

2. Experimental

$Ge_{50}Te_{50}$ and $Ge_{40}Te_{60-x}Sb_x$ system where $x = 1, 5$ and 10 were prepared in the bulk form as a mixture of Ge, Sb and Te of purity 99.999 using the conventional melt quench

*Author to whom all correspondence should be addressed.
0022-2461
DOI: 10.1007/s10853-005-5907-7

TABLE I The original bulk and final thin film compositions

Sample nomenclature	Original bulk composition	Film composition
Sb0	$Ge_{50}Te_{50}$	$Ge_{21}Te_{79}$
Sb1	$Ge_{40}Sb_1Te_{59}$	$Ge_{12.77}Sb_{1.72}Te_{85.51}$
Sb5	$Ge_{40}Sb_5Te_{55}$	$Ge_{16.15}Sb_{6.73}Te_{77.13}$
Sb10	$Ge_{40}Sb_{10}Te_{50}$	$Ge_{12.537}Sb_{5.33}Te_{82.24}$

technique. Seven grams of each sample was weighted as weight percent, then the mixture of pure elements were mixed in an evacuated sealed silica ampoule under vacuum of 10^{-5} torr. The ampoules containing the samples were then placed in a furnace whose temperature was raised in steps up to 950 ± 20°C for 18 hr. The ampoules were shaken several times to ensure the homogeneity during the synthesising process. Then, the ampoules were removed from the furnace and quenched in an ice water. The obtained samples were examined by the X-ray powder diffraction, accordingly the obtained samples are found to be crystalline.

Thin films of thickness 300, 400, 500 and 550 nm were prepared by thermal evaporation technique using an Edwards coating system E-306 with evaporation rate (15–20 Å/s). The thickness of all films was controlled using MAXTEX. Inc model TM200 Sin 351-thickness monitor. All samples were deposited on a Pyrex substrate, at room temperature (25 to 30°C) during film condensation. The final composition was determined using the Energy Dispersive X-ray (EDX) measurements. The obtained compositions are tabulated in Table I.

The amorphisity of the as-deposited thin films is checked using X-ray diffractometer (type Philips 1390) with Cu K_α-radiation and Ni-filter. The temperature dependence of a.c and d.c conductivity and thermoelectric power of as-deposited films have been studied during isochronal annealing from room temperature up to 550 k by using the coplanar, MIM, arrangement. All measurements were carried out in an evacuated Pyrex container built specially for the present work, in vacuum of less than.01 torr to reduce possible oxidation of the films.

3. Results and discussion

3.1. X-ray diffraction

Fig. 1 shows a typical X-ray diffraction patterns for all as-deposited compositions of 550 nm thickness. It is noted that, all samples are in the amorphous state where there is no characteristic diffraction peaks. This same feature was found to be the same for all the samples.

3.2. Electrical properties

3.2.1. D.C. electrical conductivity

The d.c. electrical conductivity of all as-deposited films of 400 nm thickness for all compositions were measured and plotted as a function of 1000/T as shown in Fig. 2. It is noted that, the conductivity increases gradually with

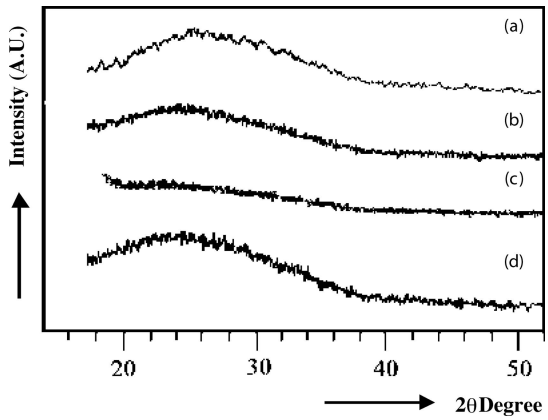

Figure 1 Representation of X-ray diffraction pattern for; (a) $Ge_{21}Te_{79}$, (b) $Ge_{12.77}Sb_{1.72}Te_{85.51}$, (c) $Ge_{16.15}Sb_{6.73}Te_{77.13}$ and (d) $Ge_{12.537}Sb_{5.33}Te_{82.24}$ at 550 nm thickness.

temperature (non-degenerate semiconductor). At a specific temperature, the conductivity abruptly increases five orders of magnitude, followed by a nearly constant value. During cooling the value of the conductivity decreases very slowly with temperature (degenerate semiconductor). It was found that, the slope is negative for all samples with different thickness, i.e. the behaviour of the electrical conductivity following the phase change is neither metallic nor semimetallic. This post transformation behaviour may be explained on the basis of the carrier concentration, n, or carrier's mobility, μ. The apparent abrupt transition of conductivity is generally may be due to the transformation from non-degenerate to degenerate semiconductor. This is confirmed by the calculation of activation energy during heating before transition and

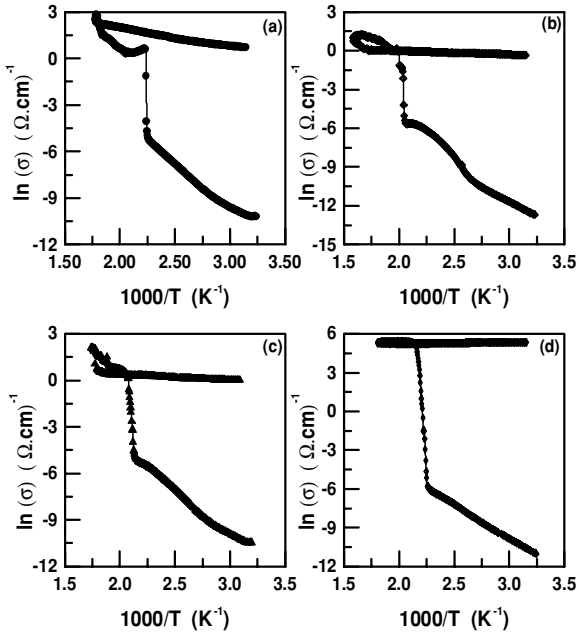

Figure 2 Temperature dependence of d.c. electrical conductivity for; (a) $Ge_{21}Te_{79}$, (b) $Ge_{12.77}Sb_{1.72}Te_{85.51}$, (c) $Ge_{16.15}Sb_{6.73}Te_{77.13}$ and (d) $Ge_{12.537}Sb_{5.33}Te_{82.24}$ at 400 nm thickness.

TABLE II d.c. electrical parameters for films

	Heating				Cooling	
Sample nomenclature	Temperature range (K)	E_{dc}* (eV)	$\ln(\sigma_0)$ $(\Omega.cm)^{-1}$	Transition temp. (K)	Temperature range (K)	E_{dc}** (eV)
Sb0	312–443	0.43	2.46	445	317–563	0.036
Sb1	309–388	0.42	3.20	485	317–630	0.040
Sb5	306–453	0.50	7.70	470	323–577	0.035
Sb10	312–443	0.43	2.46	445	317–563	0.036

E_{dc}**: activation energy of degenerate s.c. below the transition temperature; E_{dc}*: activation energy of non- degenerate s.c. post transition.

TABLE III d.c. electrical parameters for $Ge_{21}Te_{79}$ films "Sb0"

	Heating				Cooling	
Film thickness (nm)	Temperature range (K)	E_{dc}* (eV)	$\ln(\sigma_0)$ $(\Omega.cm)^{-1}$	Transition temperature (K)	Temperature range (K)	E_{dc}** (eV)
80	309–423	0.42	6.20	473	317–572	0.10
300	306–427	0.32	1.22	489	321–565	0.08
400	307–400	0.48	7.30	443	317–561	0.11
550	307–440	0.39	5.06	445	320–546	0.11

E_{dc}**: activation energy of degenerate s.c. below the transition temperature; E_{dc}*: activation energy of non- degenerate s.c. post transition.

during cooling according to the following equation,

$$\sigma = \sigma_o \exp\left(-\frac{E_{dc}}{kT}\right) \quad (1)$$

where E_{dc} is the activation energy due to d.c. conductivity and k is the Boltzmann's constant. From the above results, it is noted that, these alloys are a semiconductor material having a defect localized states separated from the Fermi level by energy E_{dc}~0.43 eV during heating process and before the transition. After transition the Fermi level is moved toward the bottom of the valance band but still within the gap, and the material behaves as a degenerate semiconductor. Table II shows that, changes of, Sb, concentration have almost no effect on the value of the activation energy. Also, it is noted that there is no significant effect on the activation energy as a function of the film thickness, indicating that the films structure structure and homogenity didn't changed. Table III present the results concerning the $Ge_{21}Te_{79}$ sample where all samples behaves' in a similar manner.

3.2.2. A.C. electrical conductivity

The measurement of the a.c. electrical conductivity, $\sigma_{tot}(\omega)$, on the other hand for the amorphous semiconductor gives an idea about the conductivity of that material as well as the relaxation behaviour. Generally, $\sigma_{tot}(\omega)$ is evaluated by; $\sigma_{tot}(\omega) = \omega C \tan(\delta)\frac{d}{A}$ where ω is the applied angular frequency, δ is the loss angle, C the measured capacitance in Farad, d is the electrodes separation and A is the sample cross section area.

While the frequency dependent electrical conductivity is given by [12];

$$\sigma(\omega) = A\omega^s \quad (2)$$

where;

$$\sigma_{tot}(\omega) = \sigma(\omega) + \sigma_{dc} \quad (3)$$

here, s, is the frequency exponent. If $\sigma_{tot}(\omega) = \sigma_{dc}$ then, the frequency dependent electrical conductivity, $\sigma(\omega)$, vanishes. The total conductivity for all compositions with different thickness are obtained by measuring the capacitance of the sample C_s and the loss tangent, $\tan(\delta)$, using a computerized RCL bridge at the specific frequencies 0.12, 1.0 and 10.0 kHz respectively. It is noted that, all total conductivity measurements take the same behaviour and value as the d.c. conductivity. Fig. 3 shows representative results for different compositions for the 400 nm thickness. When $\ln \sigma_{tot}(\omega)$ is plotted as a function of applied frequency, ln(f), for all samples it is noted that, the value of the frequency exponent, s, is equal to zero as shown in Fig. 4, for the representative Sb0 sample. This points out to that the electrical conductivity for all samples with different thickness is frequency independent in the tested frequency range.

3.2.3. Thermoelectric power

The measurement of thermoelectric power, TEP, on the other hand for semiconducting materials is a good method to determine the type of conduction depending on the sign of the Seebek coefficient, S. Additionally it is an

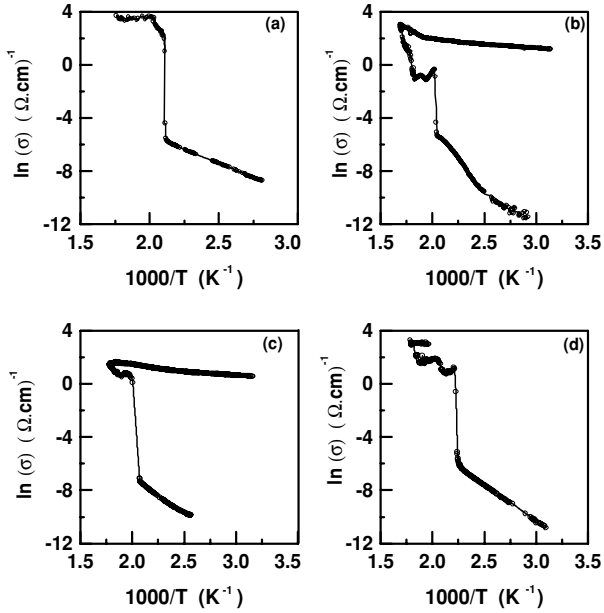

Figure 3 Temperature dependence of a.c. electrical conductivity for; (a) $Ge_{21}Te_{79}$, (b) $Ge_{12.77}Sb_{1.72}Te_{85.51}$, (c) $Ge_{16.15}Sb_{6.73}Te_{77.13}$ and (d) $Ge_{12.537}Sb_{5.33}Te_{82.24}$ with 400 nm thickness at 1.0 kHz.

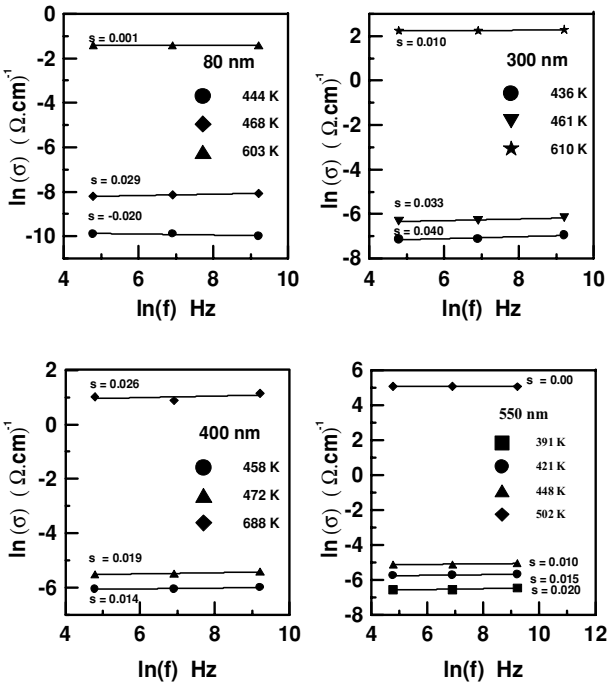

Figure 4 Representation of ln(σ) as a function of ln(f) for $Ge_{12.77}Sb_{1.72}Te_{85.51}$ films.

alternative method to calculate the optical temperature coefficient, γ, according to the formula [13];

$$E_c - E_f = E(0) - \gamma T \quad \text{or} \quad E_f - E_v = E(0) - \gamma T \tag{4}$$

where E_c, E_v and E_f correspond as usual the conduction, valance and Fermi energies, respectively. While $E(0)$ is the width of the gap at zero K.

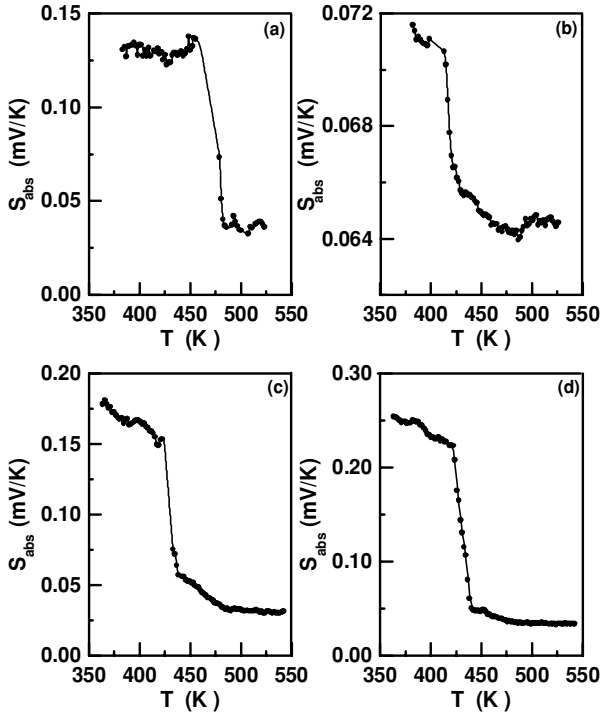

Figure 5 Temperature dependence of thermoelectric power for; (a) $Ge_{21}Te_{79}$, (b) $Ge_{12.77}Sb_{1.72}Te_{85.51}$, (c) $Ge_{16.15}Sb_{6.73}Te_{77.13}$ and (d) $Ge_{12.537}Sb_{5.33}Te_{82.24}$ with 300 nm thickness.

The TEP of the amorphous samples was measured from room temperature up to 550 K as shown in Fig. 5, for all samples with 300 nm thickness. From Fig. 5 it is noted that, the thermoelectric power is positive indicating a p-type (holes) semiconductor [13, 14], within the whole temperature range. The positive sign behaviour is preserved even above the abrupt transition.

Generally if the conduction is due to one type of carriers, then, the temperature dependence of TEP obeys the following equation [13]:

$$S = \frac{k}{e}\left[\frac{E_{th}}{kT} - \frac{\gamma}{k} + A\right] \tag{5}$$

where E_{th} is the activation energy due to TEP and A is a constant nearly equal to unity for amorphous state [13]. When TEP below the transition is plotted as a function of the reciprocal of temperature it give a straight line that has positive slope equals to E_{th}. The activation energy as calculated from the liner curves are shown in Figs. 6a–d for Sb0, Sb1, Sb5 and Sb10 samples respectively and are tabulated in Tables IV to VII respectively.

As the activation energy, E_{dc}, due to electrical conductivity below the transition temperature is compared with that of the activation energy E_{th} due to TEP, it is noted that, $E_{\text{th}} < E_{\text{dc}}$ for all samples. This inequality indicates that the conduction mechanism is due to hopping [13].

3.2.3.1. Determination of the optical temperature coefficient The optical temperature coefficient, γ, given above

TABLE IV Thermoelectric power parameters calculated for $Ge_{21}Te_{79}$ films. E_{th}: activation energy, and γ is the optical temperature coefficient as calculated from T.E.P

Film thickness (nm)	Temperature range (K)	E_{th}(eV)	$\Delta W_1 = E_{dc} - E_{th}$ (eV)	Transition temp. (K)	γ (eV/K) $\times 10^{-4}$
80	335–382	0.342	0.078	473	12.2
400	366–375	0.295	0.135	453	7.08
550	405–440	0.368	0.088	445	8.21

TABLE V Thermoelectric power parameters calculated for $Ge_{12.77}Sb_{1.72}Te_{85.51}$ films. E_{th}: activation energy and γ is the optical temperature coefficient as calculated from T.E.P

Film thickness (nm)	Temperature range (K)	E_{th} (eV)	$\Delta W_1 = E_{dc} - E_{th}$ (eV)	Transition temp. (K)	γ (eV/K) $\times 10^{-4}$
300	364–372	0.018	0.416	413	0.919
400	366–375	0.137	0.291	485	3.274
550	375–395	0.101	0.275	443	8.207

TABLE VI Thermoelectric power parameters calculated for $Ge_{16.15}Sb_{6.73}Te_{77.13}$ films. E_{th}: activation energy, and γ is the optical temperature coefficient as calculated from T.E.P

Film thickness (nm)	Temperature range (K)	E_{th} (eV)	$\Delta W_1 = E_{dc} - E_{th}$ (eV)	Transition temp. (K)	γ (eV/K) $\times 10^{-4}$
300	433–443	0.064	0.23	422	8.85
400	339–353	0.093	0.414	470	11.16

TABLE VII Thermoelectric power parameters calculated for $Ge_{12.537}Sb_{5.33}Te_{82.24}$ films. E_{th}: activation energy and γ is the optical temperature coefficient as calculated from T.E.P

Film thickness (nm)	Temperature range (K)	E_{th} (eV)	$\Delta W_1 = E_{dc} - E_{th}$ (eV)	Transition temp. (K)	γ (eV/K) $\times 10^{-4}$
300	382–400	0.118	0.227	422	1.42
400	365–389	0.126	0.325	441	2.63

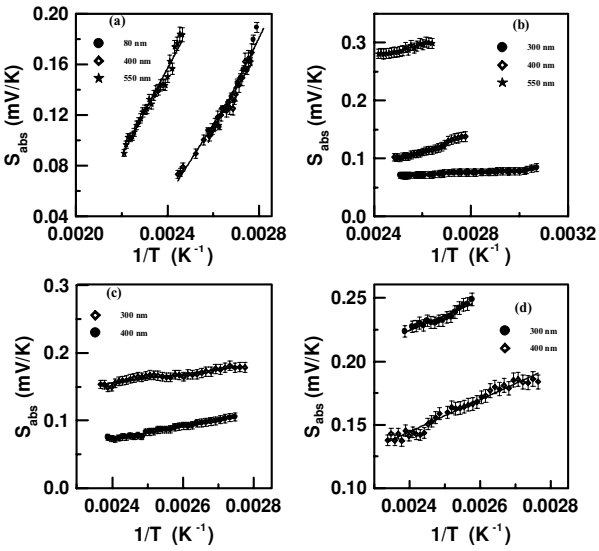

Figure 6 Absolute thermoelectric power as a function of 1/T for; (a) for $Ge_{21}Te_{79}$, (b) for $Ge_{12.77}Sb_{1.72}Te_{85.51}$, (c) for $Ge_{16.15}Sb_{6.73}Te_{77.13}$ and (d) for $Ge_{12.537}Sb_{5.33}Te_{82.24}$.

in Equation 4 can be obtained by measuring the optical absorption as a function of temperature. Alternatively, it can be calculated from the thermoelectric power through the Peltier coefficient, Π. The Peltier coefficient Π may be calculated according to;

$$\Pi = ST = -\frac{k}{e}\left[\frac{E_{th}}{k} - \frac{\gamma}{k}T + TA\right] \qquad (6)$$

The Peltier coefficient, Π , is plotted as a function of temperature for all tested samples, as shown in Figs. 7a–d. These curves show a linear dependence and having a slope equal to $-(\Pi$ /e-k/e), where, γ, is the optical temperature coefficient. The obtained values of, γ, were found to have a magnitude of 10^{-4} eV/K. This is in consistence with that reported by Moot & Davis [13] for chalcogenide materials.

3.2.3.2. Carrier concentration and carrier mobility A raised up question concerning the origin of the abrupt transition observed in the conductivity as well as in, TEP, measurements is matter of our concern. Is it due to change in the charge carrier concentration or change of the carrier mobility or change in both? To determine which of these mechanisms is the main cause of that transition; the carrier concentration and the charge mobility must be calculated first. From thermoelectric power, the free-

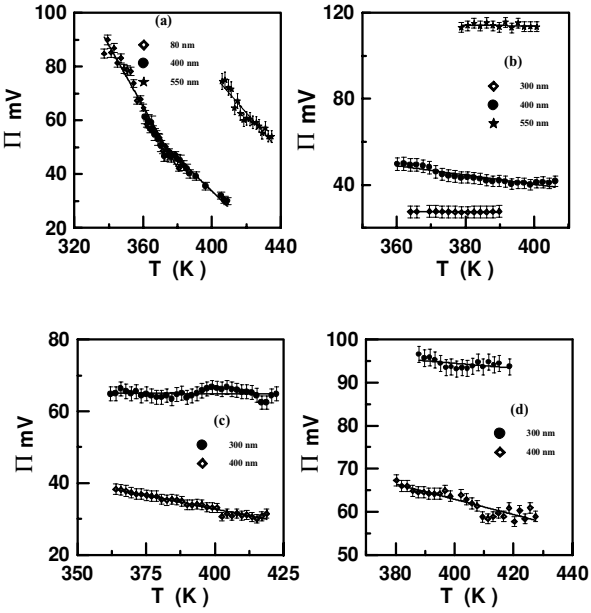

Figure 7 Peltier coefficient as a function of temperature; (a) for $Ge_{21}Te_{79}$, (b) for $Ge_{12.77}Sb_{1.72}Te_{85.51}$, (c) for $Ge_{16.15}Sb_{6.73}Te_{77.13}$ and (d) for $Ge_{12.537}Sb_{5.33}Te_{82.24}$.

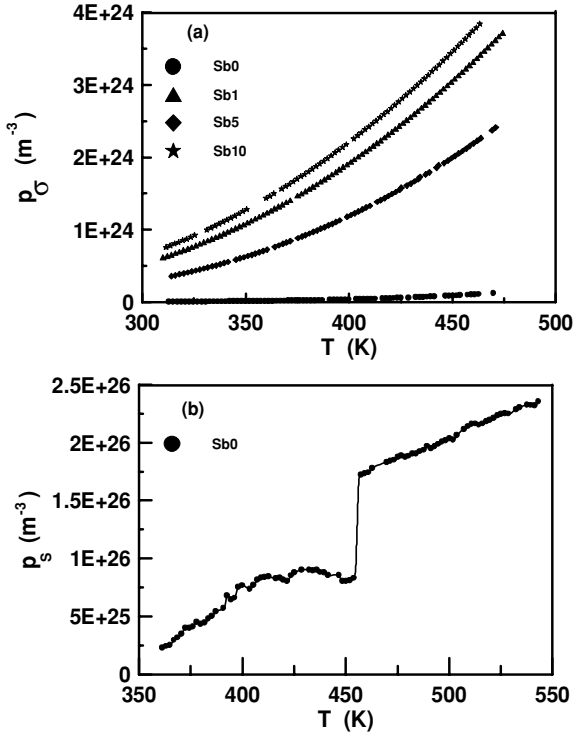

Figure 8 Representation of carrier concentration as a function of temperature that are calculated from; (a) d.c. conductivity & (b) thermoelectric power.

charge-carrier concentration can be calculate applying the following equation [15];

$$p_S = 2\left(\frac{2\pi m * kT}{h^2}\right)^{3/2} \exp\left(2 - \frac{S}{k}\right) \qquad (7)$$

Where m^* is the effective mass of charge carrier, k is the Boltzmann's constant, S is the absolute value of thermoelectric power and h is the Planck's constant. A value of $m^* = 0.76m_e$ is being used [16] for the amorphous state in the present work, where it is much less in the crystalline hexgonal phase [18]. The number of carrier concentration can also be calculated from the d.c. conductivity measurements if the thermal activation energy is known according to the following equation [17];

$$p_\sigma = 2\left(\frac{2\pi m * kT}{h^2}\right)^{3/2} \exp\left(\frac{-E_{dc}}{kT}\right) \qquad (8)$$

Where, E_{dc} is the thermal activation energy as calculated from the d.c. conductivity of the amorphous phase during heating.

On the other hand to calculate the charge mobility, μ, at different temperatures it is usually being done by calculating the free-charge-carrier concentration from independent Hall-coefficient that is connected to the conductivity. However, this may also be done by evaluating the free-carrier concentration by applying the thermoelectric power measurements Equation 7. The mobility, μ, is then calculated by correlating the electrical conductivity and TEP by applying the relation;

$$\mu = \frac{\sigma_{dc}}{p_s e} \qquad (9)$$

While the exponential temperature dependence of the mobility can be represented by the following relation [13];

$$\mu = \mu_o \exp\left(\frac{-\Delta E_\mu}{kT}\right) \qquad (10)$$

where μ_0 is the grain boundary limited mobility [14]. The carrier concentration p_σ was calculated for all samples of film thickness 400 nm below the transition temperature and the data are shown in Fig. 8a. On the other hand, the carrier concentration p_s was calculated applying Equation 7 for all samples with film thickness 400 nm at all the temperature range (below and above transition) as shown in Fig. 8b.

The charge mobility was calculated accordingly from thermoelectric power using Equations 9 and 7 respectively. Fig. 9 shows the relation between μ and the reciprocal of the absolute temperature. This points to that the transition in conductivity and/or thermoelectric power is due to abrupt increase in the charge mobility not to the carrier concentration. This results may be explained by noting that, p_s, is only changes within the same order of magnitude (10^{25} m^{-3}), while μ is changes within a wide range from 10^{-6} to 0.1(cm^2/V.s) as shown in Tables VIII and IX.

3.2.3.3. Calculation of minority carrier concentration
Fig. 8 shows that, the carrier concentration as calculated from TEP is larger than that calculated from the electri-

TABLE VIII Representation of carrier concentration parameters at 325 K, in the amorphous phase

Parameter sample	p_s (m^{-3}) $\times 10^{25}$	p_σ (m^{-3}) $\times 10^{23}$	log μ $cm^2/(V.s)$	n_{po} (m^{-3}) $\times 10^{23}$
Sb0	11.851	0.0568	−5.566	0.035
Sb1	3.1752	7.8375	−5.918	4.843
Sb5	7.9506	4.3603	−5.489	2.694
Sb10	1.6713	9.2375	−4.856	5.709

TABLE IX Representation of carrier concentration parameters at 325 K, above transition

Parameter sample	p_s (m^{-3}) $\times 10^{25}$	p_σ (m^{-3}) $\times 10^{23}$	log μ $cm^2/(V.s)$	n_{po} (m^{-3}) $\times 10^{23}$
Sb0	22.850	2.8014	−0.983	1.7310
Sb1	19.040	55.810	−1.307	34.492
Sb5	20.026	38.900	−0.974	24.042
Sb10	18.694	61.861	−0.859	38.232

cal conductivity. If the material has two types of carriers (holes and electrons) one type is a major while the other is minor as long as the alloys under study is of *p*-type. As our samples are *p*-type semiconductor, then the majority carriers are holes, p_{po}, while the minority carriers are electrons, n_{po}. Usually, thermoelectric power appears as due to a result of transfer of majority carriers, while the electrical conductivity is a final sum of the recombination of majority and minority carriers. Accordingly, the number of minority carriers can be obtained according to the mass action law [17]:

$$p_{po} \cdot n_{po} = n^2 \tag{11}$$

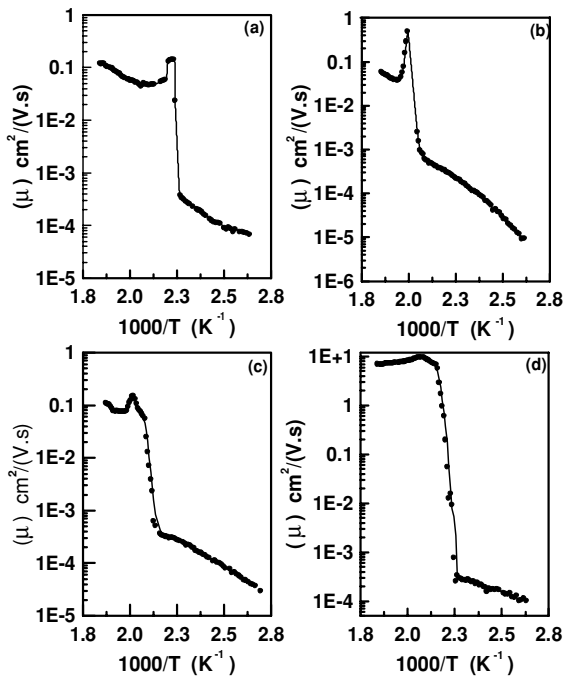

Figure 9 Representation of the calculated (μ) for; (a) $Ge_{21}Te_{79}$, (b) $Ge_{12.77}Sb_{1.72}Te_{85.51}$, (c) for $Ge_{16.15}Sb_{6.73}Te_{77.13}$ and (d) for $Ge_{12.537}Sb_{5.33}Te_{82.24}$ at 400 nm thickness.

where n is the intrinsic current carriers which can be considered as that calculated from the d.c. conductivity p_σ If p_{po} is proposed equal to p_s which can be expressed as in the following equation;

$$p_s = n_{po} + p_\sigma \tag{12}$$

When Equations 11 and 12 are combined with each other, Equation 11 becomes;

$$\left(n_{po} + p_\sigma\right) n_{po} = p_\sigma^2 \tag{13}$$

then;

$$n_{po}^2 + p_\sigma n_{po} - p_\sigma^2 = 0 \tag{14}$$

Then, to obtain the number of minority carriers n_{po} according to the following equation obtained by solving Equation 14 [17];

$$n_{po} = \frac{-p_\sigma + \sqrt{p_\sigma^2 + 4p_\sigma^2}}{2} = \frac{p_\sigma\left(\sqrt{5} - 1\right)}{2} \tag{15}$$

The calculated free-charge carriers that were evaluated from the TEP, d.c. conductivity, mobility and the number of minor current carriers below transition are shown in Table VIII at 325 K, and above the transition temperature namely at 531 K as shown in Table IX. Tables VIII and IX respectively show that the numbers of majority carriers p_s is 10^2 times greater than the numbers of minority carriers n_{po}. Also the charge carrier mobility shows a great change post the transition, since μ changes within the range of 10^{-6} to 0.1 cm^2/V.s.

4. Conclusion

From the above results, it is noted that, the temperature dependence of the electrical conductivities of the $Ge_{50-x}Sb_yTe_{100+x-y}$ thin films was found to have an irreversible abrupt transition at about 450 to 470 K. Thermoelectric power measurements on the other hand revealed that, these alloys are *p*-type semiconductors even above the transition. Calculation of the free-charge carrier concentration and its mobility's shows that, the abrupt transition appears in thermoelectric power as will as in the conductivity is due to an abruptly change in the carrier mobility.

References

1. L. MEN, J. TOMINAGA, H. FUJI and N. ATODA, Oxygen doping effects on super-resolution scattering-mode near-field optical data storage. *Jap. J. Appl. Phys.* **39** (2000) 2639.
2. N. YAMADA, E. OHNO, K. NISHIUCHI, N. AKAHIRA and M. TAKAO, Rapid-phase transition of GeTe-Sb_2Te_3 pseudobinary amorphous thin films for an optical disk memory. *J. Appl. Phys.* **69**(5) (1991) 2849.

3. S. YAMANAKA, S. OGAWA, I. MORIMOTO and Y. UESHIMA, Electronic structure and optical properties of GeTe and $Ge_2Sb_2Te_5$. *ibid*. **37** (1998) 3327.
4. K. L. CHOPRA and S. K. BAHL, Amorphous versus crystalline films. I. growth and structural behaviour. *J. Appl. Phys*. **40**(10) (1969) 4171.
5. *Idem.* Amorphous versus crystalline films. III. Electrical properties and band structure. *ibid*. **41**(5) (1970) 2196.
6. K. N. MADHUSOODANAN, J. PHILIP, G. PARTHASATHY, S. ASOKAN and E. S. R. GOPAL, Optical absorption and thermal diffusivity in Ge_xTe_{100-x} glasses by the photoacoustic technique. *Phill. Mag. B* **58**(1) (1988) 123.
7. S. R. OVSHINKY, Optically induced phase change in amorphous materials. *J. Non-Crys. Solids* **141** (1992) 200.
8. SANG Y. KIM, SANG J. KIM, HUN SEO and R. MYONG KIM, Complex refractive indices of GeSbTe-Alloy thin films: effect of nitrogen doping and wavelength dependence. *Jap. J. Appl. Phys*. **38** (1999) 1713.
9. F. JAN and H. RUAM. Optical properties of some organic and inorganic thin films in an abnormal dispersion region and their application, and references their in. in Fourth International Conference on Thin Films *Physics and Applications*. **4086**: pp. 1 to 6.
10. B. J. KOOI, W. M. G. GROOT and J. TH. M. DE HOSSON, In situ transmission electron microscopy study of the crystallization of $Ge_2Sb_2Te_5$. *J. Appl. Phys*. **95**(3) (2004) 924.
11. D. WAMWANGI, W. K. NJOROGE and M. WUTTIG, Crystallization kinetics of $Ge_4Sb_1Te_5$ films. *Thin Solid Films* **408** (2002) 310.
12. S. R. ELLIOTT, A. c. conduction in amorphous chalcogenide and pnictide semiconductors. *Adv. phys*. **36**(2) (1987) 135.
13. N. F. MOTT and E. A. DAVIS, Electronic processes in non-crystalline materials, Chapter "7" (Clarendon Press, Oxford, 1971).
14. K. L. CHOPRA and S. K. BAHL, Thermoelectric power behaviour of amorphous versus crystalline Ge and GeTe films. *Thin Solid Films* **12**(2) (1972) 211.
15. Z. H. KHAN, M. ZULFEQAUR, A. KUMAR and M. HUSAIN, Electrical conductivity and thermoelectric power of a-$Se_{80-x}In_x$ and $Se_{80-x}Ge_{20}In_x$ thin films. *Can. J. Phys*. **80** (2002) 19.
16. I. A. AVRAMOVA and S. K. PLACHKOVA, Density-of-states effective masses in the system $Ge_{1-x}Ag_{x/2}Bi_{x/2}Te$ ($0 < x < 0.333$). *J. Phys.: Condens. Matter.* **11** (1999) L469.
17. G. YEPIFANOV, Physical principles of microelectronics, Chapter "6" (Mir Publisher, Moscow, 1974) pp. 148.
18. A. MENDOZA-GALVA'N and J. GONZA'LEZ-HERNA'DEZ, Drude-like behavior of Ge:Sb:Te alloys in the infrared. *J. Appl. Phys*. **87**(2) (2000) 760.

Received 21 March
and accepted 27 July 2005